Tuning electrical conductivity in AlN-based ceramics by incorporating graphene

Driss Kenfaui, Sophie Guillemet-Fritsch, Zarel Valdez-Nava, Lionel Laudebat, Christophe Tenailleau, Pascal Dufour, Marie-Laure Locatelli

Tuning electrical conductivity in AlN-based ceramics by incorporating graphene therein

Driss Kenfaui[1,2], Sophie Guillemet-Fritsch[1], Zarel Valdez-Nava[2], Lionel Laudebat[2,3], Christophe Tenailleau[1], Pascal Dufour[1], Marie-Laure Locatelli[2]

[1] CIRIMAT (Centre Inter-universitaire de Recherche et d'Ingénierie des Matériaux), Université de Toulouse, CNRS, INPT, UPS, 31062 Toulouse cedex 9, France.
[2] LAPLACE (Laboratoire Plasma et Conversion d'Energie), Université de Toulouse, CNRS, UPS, INP, 118 route de Narbonne, 31062 Toulouse cedex 9, France.
[3] Université de Toulouse, Institut National Universitaire Champollion, Place de Verdun 81012 Albi Cedex, France.

Abstract

Aluminum nitride (AlN) is the material of choice for high power modulus substrates. However, due to the strong covalent bonds in the AlN system and the low diffusion coefficient of its constituent elements, additives have to be used as sintering aids, typically Y_2O_3, to achieve nearly full material density. The thermal and electrical conductions can be also fostered by adding CaF_2 and carbon particles, respectively. In this paper, we report on tuning the electrical conduction within AlN-based composites developped by incorporating graphene nanoplatelets (GNP) into the AlN-based ceramics comprising the Y_2O_3 and CaF_2 additives. GNP were produced by exfoliation of graphite in isopropyl alcohol. These composites were prepared by Spark Plasma Sintering (SPS) through a new configuration called "multiple preparation" with a view to fabricating three samples per SPS cycle, revealing potential time and energy savings. A magnitude of 10 order of magnitude higher as compared to the commercial AlN was obtained for these composites by adjusting the amount of GNP as well as the way of exfoliation to produce them. This work paves the way for the development of novel multifunctional ceramic composites for Power Electronics applications.

1. Introduction

In Power Electronics (PE), the substrate has to perform concomitantly the dual functions of electrical insulation and thermal conduction. It also ensures the mechanical reliability of the arrangement of heterogeneous materials constituting the power module. Owing to their physical and mechanical properties, the Al_2O_3, AlN and Si_3N_4 ceramics are the substrates that are capable of fulfilling these functions in a PE module.

However, only Al_2O_3 and AlN ceramics are selected for high power applications because of their higher breakdown voltage and thermal conductivity,[1] with a preference for the AlN material which displays the best compromise of both properties. Si_3N_4 ceramics are less suitable due to higher manufacturing cost.

These ceramics currently fulfill the multiple functions of the substrate in the traditional Si-based PE systems. They will nonetheless undergo stronger electrical field in new SiC-based systems operating under higher voltages. Their functional and mechanical properties must therefore be controlled and/or improved locally and/or in terms of volume in order to cope with more severe stresses arising both from operation (a rise in voltage and temperature) and integration. In other words, a new generation of substrates should be developed to take advantage of the high potential offered by large gap semiconductors.

Thus, AlN ceramics turn out to be the best-suited existing substrates to face those challenges[2–4] due to their excellent aforesaid attributes.[5,6] The production of dense AlN ceramics by conventional sintering requires however high temperature levels associated with long dwell time. Indeed, these materials weakly densify under the sole action of heat due to the strong covalent bonds in the AlN system and the low diffusion coefficient of their constituent elements.[2–4] Long sintering time and high temperature levels not only cause an increase in the cost of production but also promote the grain growth of which leads to the degradation of the mechanical properties of the sintered ceramics. Spark Plasma Sintering (SPS), well-known for its ability to accelerate the kinetics of sintering,[5] is today the most widely used method for producing highly dense AlN ceramics in very short times.[2,3,6]

Nevertheless, the addition of a limited fraction of sintering additives (rare earths and/or alkaline earth oxides) is essential to promote the densification of AlN materials by creating a liquid phase,[3,4,6] and to improve their thermal conductivity by reducing the oxygen impurities

present therein.[7] AlN particles are usually covered with a thin layer of Al_2O_3 oxide (1-2%) which reacts with the sintering additives (e.g. Yttrium oxide Y_2O_3) and AlN powder. This results in the formation of oxides (yttrium aluminate garnet $Y_3Al_5O_{12}$ (YAG), yttrium-aluminum perovskite $YAlO_3$ (YAP), monoclinic yttrium-aluminum $Y_4Al_2O_9$ (YAM), etc.), which fosters sintering in liquid phase of the AlN material during the sintering process.

A lot of work has therefore been reported on the heterogeneous ceramics (AlN + Y_2O_3), developed by SPS method, exhibiting a strongly densified microstructure with compounds (YAG, YAP, YAM and/or other oxides) concentrated at the grain boundaries. He *et al.*[4] reported almost complete densification (> 99%) of AlN + 3 wt% Y_2O_3 ceramics sintered by SPS under a controlled nitrogen atmosphere at 1800°C under an uniaxial pressure of 40 MPa for 10 min. These materials present a microstructure in which the oxide $YAlO_3$ is incorporated into the grain boundaries of the AlN matrix. However, this secondary phase appears thick and partially covers the AlN grains, which is prohibitive for the thermal conductivity of these materials due to the diffusion of phonons at the AlN / $YAlO_3$ interfaces.

It has also been reported that the addition of calcium fluoride CaF_2 (melting temperature of 1418°C) to the AlN + 3 wt% Y_2O_3 mixture leads to the formation of an additional oxide $Ca_3Al_2O_6$ and other products which evaporate during SPS sintering, reducing then the amount of secondary phases at the grain boundaries.[4] The reduction in the Y_2O_3 fraction in favor of CaF_2 lead to a microstructural with the secondary phases occupying only the junctions and concentrating at the triple points between the grains, thereby enhancing the thermal conduction in AlN ceramics. Moreover, Nakano *et al.*[8] reported that the thermal conduction in an AlN ceramic depends both on the different constituent phases, and on the distribution of secondary phases within the microstructure. Hence, the overall thermal conductivity of the heterogeneous ceramic could be increased if the microstructure includes reduced amount of secondary phases located preferentially at the triple points between the grains and evenly distributed in the AlN matrix. We therefore expect that the thermal conductivity of AlN + 1% m Y_2O_3 + 2% m CaF_2 ceramics will be higher as compared to the AlN + 3% m Y_2O_3 and AlN ones.

On the other hand, little work has been reported on the electrical properties of AlN-based ceramics, especially the electrical conductivity (σ). Indeed, it is only in the last few years that the graphene nanoplatelets (GNP) have been incorporated in the AlN microstructure in order to amend its σ.[9,10] The choice of this additive is driven by the advantages of a large specific

surface area and high charge carrier mobility of the graphene sheets, but also by its exceptional mechanical properties[11] which give GNP a high resistance to irreversible damage at high temperature under mechanical stress such as during SPS processing, thereby distinguishing them from carbon nanotubes (CNT).[12,13] CNT have indeed been reported to be reactive with oxides and nitride-based materials at high temperature, making it difficult to maintain their structure during SPS sintering.[14] GNP also exhibit thermal conductivity (κ~ 6-10 $Wm^{-1}K^{-1}$) higher with two orders of magnitude compared to reduced graphene oxide (rGO).[15,16] Note that rGO is obtained by the reduction of the graphene oxide (GO) during sintering of AlN.[17]

The most frequently techniques used for producing GNP are:[18-20]

i) Physical exfoliation of graphite using adhesive tape, which leads to the production of graphene in small area, but with the presence of residues duct tape on it.

ii) Epitaxy of graphene from silicon carbide (SiC), or the oriented growth, that requires the use of a high vacuum, a source of SiC as well as very high heating temperatures (~ 1300°C) to evaporate the silicon atoms, then the carbon atoms will rearrange themselves to form layers of graphene.

iii) Heterogeneous catalysis using chemical vapor deposition (CVD) which allows forforming graphene on a large surface, on copper or nickel supports. This method also involves the use of high temperatures and low pressures, hence a high cost.

iv) Exfoliation of graphite in liquid phase.[20]

Simsek *et al.* [9] employed the last technique (*iv*) to produce GNP by exfoliating the graphite in isopropyl alcohol using the conventional ultrasound. The obtained GNP were then incorporated within based-AlN matrix to elaborate ceramic composites (AlN + 2.9 wt% Y_2O_3 + x vol% GNP) by SPS at 1700 - 1750°C under a uni-axial pressure of 50 MPa for 5 min under a controlled nitrogen atmosphere. An almost full composite density (> 99%) was achieved for the volume fractions x ≤ 5 vol% of GNP, but it dropped slightly to 97.8% for x = 10 vol%. The evolution of σ with x revealed that σ can be increased from $\sigma = 10^{-14}$ $S.cm^{-1}$ for a ceramic with no GNP up to 1 $S.cm^{-1}$ for the composite containing 10 vol% of GNP.

In the light of the state of the art drawn up above, we decided to develop the ceramic composites AlN + 1 wt% Y_2O_3 + 2 wt% CaF_2 containing a GNP fraction of 2.5 and 10 vol% by

SPS. The GNP were produced by exfoliation of graphite in isopropyl alcohol using two exfoliation methods: conventional sonication (ultrasonic bath) and sonotrode.

These composites were fabricated under the same SPS conditions in order to assess the contribution of the selected additives. They were particulary elaborated using "multiple preparation configuration" with the aim of fabricating three samples per SPS cycle. It enabled to have the number of samples needed to perform different material characterizations and to assess the degree of reproducibility. Their microstrcutres features and electrical conductivity were compared with those of the ceramics AlN, AlN + 3 wt% Y_2O_3 and AlN + 1 wt% Y_2O_3 + 2 wt% CaF_2. Note that the reference and the description of the samples are summarized in Table 1.

2. Experimental section

2.1. Powder preparation and shaping

The AlN powder (Atochem, France), with a median grain size d_{50} = 1.9 µm, and the sintering additives Y_2O_3 (purity: 99.9%, Shinetsu, Japan) and CaF_2 (purity: 99.7%, Alfa Aesar, Germany) were selected as the starting precurssors. The respective fractions of Y_2O_3 and CaF_2 were set at 1 and 2 wt% with a goal of reaching nearly full densification concomitantly with improving the thermal conductivity of AlN-based materials.

To tune the electrical conduction, GNP were chosen for their aforementioned advantages. Two methods of exfoliation were tested to produce them: ultra sonic bath and sonotrode.
The first batch of GNP were produced by exfoliation of 2.5 vol.% of graphite (median lateral particle size: 15 µm, Skyspring Nanomaterials, Inc. - USA) in 20 ml of isopropyl alcohol using a classical ultra sonic bath. The choice of this liquid dispersant is governed by its evaporation temperature (82.6°C) which is much lower than that of (NMP) N-methyl-2-pyrrolidone (202°C) or (DMF) N, N-dimethylformamide (153°C), solvents known for their greater ability to stabilize the dispersion of graphene sheets produced by exfoliation of graphite.[20] Indeed, such a low evaporation temperature is required to be able to separate more easily the solvent from the final powder mixture. This separation is carried out by evaporating the solvent using the rotary evaporator as describted later in this section.
However, the GNP, produced by the conventional sonication (ultrasonic bath), are still stacks comprising a very high number of graphene sheets. However, the effects of graphene at the

electronic, and therefore electric, level are more prominent in the quantum domain, that is, when the thickness of the graphene layers is close to the mean free path of the electron. In practice, below ten layers of graphene, the electrical effects significantly increase.

We therefore decided to use the sonotrode, a probe sonicator (Sonics Materials VCX-750, Fisher Scientific, France) fitted with a high-frequency ultrasonic generator, to sonicate a similar liquid solution comprising 2.5 vol.% of graphite in 20 ml of Isopropylic alcohol. The sonicator was set to a power of 150 W with an amplitude of 40% and a pulsed mode of the cycle 4s ON (sonication) / 6s OFF (pause). The aim was to provide the required energy to exceed that of Van der Waals type bonding between the graphene sheets for the purpose of exfoliating the graphite.

The pause time allows to limit the rise in temperature of the solution and therefore to slow its evaporation . The solution volume was then kept constant throughout the sonication time. The solution was sonicated for 2 h; the total time of the sonication experiment was 5 h taking into account the total pause time. It was thereafter left to settle with a view to evidencing the graphite exfoliation. Figure 1 shows an image taken 15 h after the solution sample was sonicated. The volume Va (black part of the container) is visibly higher than that of the solution before sonication, suggesting exfoliation of the graphite.

This result was also obtained for two similar solutions previously subjected to effective sonication times of 0.5 and 1 h. The apparent volumes V_a, obtained after these solutions were left to settle for 15 h, were compared. The longer the sonication time, the better the exfoliation. The solution, with the highest volume, was thereafter subjected to 3 additional sonication tests of 2 h each. The volume V_a continued to increase indicating a more exfoliation of the graphite.

On the other hand, the powder mixture AlN + x1 wt% Y_2O_3 + x2 wt% CaF_2 was homogenized in absolute alcohol using a mechanical mixer adjusted to a rotation of 200 rpm for 1 h. The powder was then heated at 80°C for 15 h to remove the solvent.

Then, this powder was introduced with GNP dispersed in isopropyl alcohol into a glass flask fixed in a rotary evaporator. The flask was subjected to a rotation of 70 rpm for 2 h to homogenize the resulting solution. It was heated up to 70°C under vacuum to reduce the partial pressure of the solvent. The produced vapor was condensed after being pipped to the cooling system, and the liquid solvent was finally conveyed to a recovery tank.

The resulted powder mixure was shaped in the SPS apparatus (Dr. Sinter 2080 device from Sumitomo Coal Mining – Fuji Electronic Industrial, Saitama, Japan). It was first loaded into a graphite mold of 20 mm in diameter. A graphite sheet was previously placed on the internal wall of the mold in order to avoid any reaction between it and the material, on the one hand, and to facilitate the demolding of the sample after sintering, on the other hand. The mold was then transferred to the SPS and heated up to 1800°C for 10 min, at a rate of 100°C/min, under uniaxial pressure of 50 MPa and nitrogen atmosphere. Such experimental conditions for SPS shaping were seleced from the literature[4,9] with the aim of achieving complete densification and limiting grain growth.

It is worth noting here that in addition to the simple preparation, *i.e.* one pellet per SPS cycle (Figure 2a), we also performed the multiple preparation of samples that involves the elaboration of three pellets per SPS cycle. The required quantity of powder for each pellet was placed between two graphite discs in the matrix as illustrated in Figure 2b, which allows then the preparation of three samples by applying only a single SPS cycle. Figures 2c-d show, for instance, the microstructures of the AY samples elaborated using simple preparation and multiple one at top, middle and bottom positoins. They evidence almost similar microstrctural features with no significant difference between the samples. Note that the AY microstructure is described later in detail (§ 3.2.1).

The multiple preparation, proposed for the first time to our knowledge, has the merits of producing, in a very short time, the number of samples required to carry out different material characterizations, on the one hand, and to evaluate the degree of reproducibility of the results obtained, on the other hand. This testifies to the relevance of such approach in terms of not only the higher production of the sintered material but also the triple saving of time and energy.

2.2. Characterization techniques

After being sonicated for 8 h as mentioned above, the solution (2.5 vol.% of graphite in 10 ml of isopropyl alcohol) was sonicated for an additional time of 1 h. Immediately after this operation, a few drops loaded with exfoliated graphite were poured onto a perforated carbon grid. It was then transferred into the transmission electron microscope (TEM) for observation (HT-7700 Hitachi 120 kV). The accelerating electron voltage was set at 80 kV to reduce the

damage that could be induced by the electron beam on the graphene while maintaining the image resolution of the particle fringes in order to distinguish the number of platelets and the local thickness on the folded edges.

The microstructure of the elaborated AlN-based materials was examined by means of the Scanning Electron Mircoscope (SEM JEOL JSM6510LV). Their chemical composition was determined by using X-ray diffractometer (Bruker D4).

The dielectric properties were probed at 20°C under low voltage (3 V_{PP}) in the 10^{-1} -10^{6} Hz frequency range for the prepared samples by the mean of a broadband impedance analyzer (Novocontrol Alpha-A). The SPS-sintered pellets of 20 mm in diameter were initially mirror-polished and annealed at 150°C during 5 h to remove all traces of water. A 80 nm-thick gold electrode was then deposited by sputtering on both faces of each sample. The metalized pellet was finally placed into the measuring cell between two conducting electrodes to form a parallel capacitor.

3. Results and discussion

3.1. Observation of GNP

TEM characterization, performed for the solution sonicated for 9 h, revealed the presence of a large number of two-dimensional and quasi-transparent platelets (Figure 3a) depicting nano-scale thicknesses and lateral sizes in the range of 600 - 2000 nm, similar to those reported elsewhere[20] for monolayers of graphene obtained by exfoliation of graphite in the solvent NMP (N-methyl-2-pyrrolidone). Generally, the observed GNP have straight edges and corners with distnguished angles allowing to perceive their nano-scale thickness, and even to forecast the very small number of monolayers. TEM images, presented in Figure 3a and b, are similar to those of graphene monolayers reported elsewhere.[20–22] We have also noted the presence of less transparent and thicker platelets as shown in Figure 3b. These platelets therefore include a higher number of monolayers.

3.2. Microstrcture and chemical compositon of the SPS-sintered materials

3.2.1. Ceramics A, AY and AYC

Figure 4a depicts the SEM image of the cross section (fractured surface) obtained by cleavage of the AlN material (sample A) produced by SPS under the aforementioned conditions. It shows a homogeneous microstructure with a density higher than 98% refelecting the relevance of the selected sintering conditions. Such microstructure comprises micro-sized grains with no significant growth occurred during the sintering, due to the very short time of the SPS processing, and no secondary phase that can be visibly distinguished at the grain boundaries. However, X-ray diffraction analyzes (Figure 4b) revealed the presence of traces of $Al_9O_3N_7$, $Al_8O_3N_6$ and $Al_{10}O_8N_3$ oxides, very likely due to the reaction of oxygen impurities with AlN during sintering.

The SEM observation of the AY ceramic (Figure 4c) shows the typical microstructure of AlN materials produced by SPS with sintering additives: the secondary phases (clear contrast) are located at the grain boundaries of the AlN matrix (dark contrast). A highly dense microstructure exceeding 99% with very limited grain growth is noted as well. Unlike the sample A (Figure 4a), the sintering is carried out in the liquid phase formed following the reaction of Y_2O_3 with AlN and Al_2O_3 present on the surface of the grains. The secondary phase, produced in liquid form during sintering, therefore flows at the grain boundaries and solidifies during cooling, thus contributing to densifying the material. Chemical analyzes indicate that its composition is close to that of YAP as shown by the XRD analysis given in Figure 4d. However, the addition of 3 wt% Y_2O_3 led to the formation of a relatively high amount of YAP which partially covers the AlN grains. This might promote phonon scattering at the YAP / AlN interfaces and consequently degrade the thermal conduction in the material. These results are in agreement with those reported by He *et al*.[4]

The micrograph of the SPS-sintered AYC ceramic is presented in Figure 4e. It evidences a homogeneous microstructure with hexagonal grains having rounded edges. The density of this material is comparable to that noted for the AY one. Nevertheless, the AYC ceramic includes much smaller amount of secondary phases at the grain boundaries, present along the junction and concentrated at the triple points between the grains. This is attributed not only to the lower fraction of the added Y_2O_3 but also to the formation of secondary phases which evaporate during sintering as evidenced by the traces in clear contrast observed on the '*spacers*' at the end of the SPS process. The X-Ray analysis shows the presence of YAP as well, coexisting however with an additional oxide $Ca_3Al_2O_6$. This based-AlN matrix was used for

fabricating the composites presented later. Its recorded X-Ray diffractogram is then similar to that given in Figure 6c.

The reduction of secondary phases within this matrix can be explained as flowes: since the decomposition temperature of CaF_2 (1418°C) is lower than the used dwell temperature (1800°C), the following chemical reactions took place during the treatment of the AlN + 1 wt%Y_2O_3 + 2 wt%CaF_2 powder mixure by SPS:[4,7]

$$6\ CaF_2 + 2\ AlN + 2\ Al_2O_3 \rightarrow 4\ AlF_3 + Ca_3Al_2O_6 + Ca_3N_2$$

$$36\ CaF_2 + 2\ AlN + 2\ Al_2O_3 + N_2 \rightarrow 24\ AlF_3 + Ca_3Al_2O_6 + 3\ Ca_{11}N_8$$

As the evaporation temperature of the AlF_3, Ca_3N_2 and $Ca_{11}N_8$ products is lower than 1800°C, they therefore evaporated during the SPS sintering.

3.2.2. Composite AlN + 1 wt% Y_2O_3 + 2 wt% CaF_2 + 2.5 vol.% GNP (AYC2.5G)

Figure 5 shows the SEM images of the fractured surfaces obtained by cleavage of the composite AYC2.5G elaborated by SPS. The GNP incorporated in this material were previously produced by exfoliation of graphite in isopropyl alcohol using conventional sonication (ultrasonic bath) for 1 h as reported by Simsek et al.[9] The microstructure seems to be not disturbed by the presence of GNP (Figure 5a) indicated by yellow arrows. It displays a density (99%) as high as that recorded for ceramics free of GNP (Figures 4), regardless of the used configuration (simple or multiple) shown in Figure 2. GNP appear to be distributed throughout the AlN matrix. However, we cannot confirm the uniformity of this distribution from SEM observations because graphene monolayers, or GNP including a very small number of graphene sheets, are very difficult to observe using SEM. High-magnification microstructural examination reveals that the in-plane of the GNP platelets tends to be perpendicular to the axis of the SPS pressing axis (Figure 5b). We also observe that GNP are inserted between the grains and follow the contours of the latter, producing ripples without fracture, thus testifying of the high mechanical resistance of graphene at high temperature under loading. We note, however, the presence of several thick GNP stacks containing a very large number of graphene layers (Figure 5c), which indicates the insufficiency of conventional sonication to produce GNP comprising a reduced number of layers. As in the case of the AYC ceramic (Figure 4e), the

secondary phases, produced in reduced quantity, are concentrated at the triple points between the hexagonal grains of the AlN. These phases, illustrated in clear contrast, are indicated by red arrows (Figure 5b). The results of the local EDS microanalyses, given in the inset of this Figure, indicated the presence of the elements Y, Al, O and Ca, supporting then those of the characterization by X-Ray diffraction which revealed the presence of YAP and $Ca_3Al_2O_6$.

3.2.3. Composite AlN + 1 wt%Y_2O_3 + 2 wt%CaF_2 + 2.5 vol.% GNP (AYC2.5GSO)

Figure 6a shows the fractured surface of the ceramic composite AYC2.5GSO fabricated by SPS. In this case, the incorporated GNP were obtained by exfoliation of graphite in isopropyl alcohol after sonication for 9 h using the sonotrode. Unlike the previous composite sample (Figure 5a), the microstructure is nearly full densified (99%) whatever the used configuration (Figure 2), but revealed little GNP, which bodes well for the presence of graphene monolayers and GNP containing a very small number of layers which are difficult to observe using SEM. This result is consistent with the TEM observations and highlights much better exfoliation of graphite by sonotrode. Examination at high magnification of the observed GNP (Figure 6b) also showed that they include a smaller number of layers as compared with the previous ceramic (Figure 5c). They are introduced between the grains and also follow the contours of the latter by exposing waves without fracture.

The local EDS microanalyses combined with the characterization by X-ray diffraction (Figure 6c) showed the presence of the oxides YAP and $Ca_3Al_2O_6$ concentrated at the grain boundaries (Inset of Figure 6a).

3.3. Electrical conductivity of the elaborated AlN-based materials

Figure 7a presents a comparaison of the frequency dependence of the electrical conductivities σ (f) measured at 20°C for the AlN material prepared by SPS (sample A) and for the commercial ceramic from Impak company. The commercial sample appears to be more resistive, as is evident from the σ shift towards lower values in the 0.5 - 5 x 10^5 Hz frequency range. At 0.1 Hz, σ is lower with an order of magnitude as compared to the A ceramic prepared by SPS (Table 2). This difference is probably tied to the oxides detected therein (Figure 4a) . It underlines the necessity to incorporate sintering additives in the AlN matrix so as to remove

oxygen impurities during sintering, thereby avoiding the formation of these oxides and, subsequently, decreasing σ.

Figure 7b shows the σ (f) curves recorded at 20°C for the composites AlN + 1 wt% Y_2O_3 + 2 wt% CaF_2 + 2.5 vol.% GNP produced by SPS using single (AYC2.5G) and multiple (AYC2.5G-H and AYC2.5G-M) configurations. For comparison, the curve σ(f) recorded for the ceramic comprising a fraction of GNP as high as 10 vol.% (AYC10G) is also plotted. The GNP incorporated in these samples were previously produced by exfoliation of graphite in isopropyl alcohol using conventional sonication (ultrasonic bath) for 1 h. The curves σ (f) of the A ceramic and of the commercial one are also given. The conductivity σ of the sample AYC10G is independent on the frequency (~ 6.5 x 10^{-2} S.cm^{-1}), which approves the choice of GNP to modify σ within AlN ceramics. The samples comprising 2.5 vol.% GNP, although shaped under the same conditions in the SPS apparatus, show visibly dispersed σ values and their electrical behaviors differ from each other. Indeed, the sample AYC2.5G presents a monotonic decrease in σ from 1 x 10^6 to 10^{-1} Hz, corresponding to a capacitive behavior that is similar to that noted for the commercial AlN material and for the A ceramic (Figure 7a). The sample AYC2.5G-Mexhibits a similar behavior in the 2 x 10^3 - 10^6 Hz range, and its σ clearly becomes less frequency dependent in the 0.1 – 2x 10^3 Hz range by showing a plateau, characteristic of a resistive behavior. It is also observed for the sample AYC2.5G-H over the entire explored frequency range. At 0.1 Hz, the σ values recorded for these last three samples are 1.7 x 10^{-12}; 2 x 10^{-9} and 1.5 x 10^{-6} S.cm^{-1} (Table 2), respectively. Such dispersion, in terms of σ as well as of the electrical behaviors, evidences that the electrical effect of GNP is different within the last three samples. This can be attributed to either a non-uniform distribution of GNP in the prepared mixture AlN + 1 wt% Y_2O_3 + 2 wt% CaF_2 + 2.5 vol% GNP, or the difference in the quality of the exfoliated GNP contained in each sample.

The curve σ(*f*) recorded at 20°C for the composites AYC2.5SO produced by SPS using simple (AYC2.5GSO) and multiple (AYC2.5GSO-H, AYC2.5GSO-M and AYC2.5GSO-L) configurations are given in Figure 7c. GNP incorporated in these samples were obtained by exfoliation of graphite in isopropyl alcohol upon sonication for 9 h using the sonotrode.

The curves σ (*f*) of the A ceramic and of the commercial sample are also plotted for comparison. We note that the composites show frequency-insensitive electrical conductivity, indicating resistive behavior over the entire explored frequency range. The samples, prepared

following multiple configuration, display almost identical values, revealing a remarkably high degree of reproducibility. They indicate a σ value close to 10^{-4} S.cm^{-1}, emphazing an increase of approximately 10 orders of magnitude as compared to the commercial sample and of the AlN ceramic produced by SPS. In addition, this value is markedly higher than the σ values noted for the previous ceramics (Figure 7b), comprising the same fraction of GNP obtained by conventional sonication of graphite. This increase in σ is very likely related to the presence of a high number of graphene monolayers with a higher mobility of charge carriers, which induces more marked electrical effects in the AlN ceramic. It may also result from a better distribution of GNP in the composites. The AYC2.5GSO sample, produced by single configuration, exhibits similar electrical behavior and a σ value of 10^{-5} S.cm^{-1}, close to that of the AYC2.5G-H, AYC2.5G-M, AYC2.5G-L (low position) samples. These results are consistent with the MET and SEM observations, and present, to our knowledge, a degree of reproducibility never reported so far for AlN-based composites containing conductive additives such as GNP. However, the values obtained (10^{-4}-10^{-5} S.cm^{-1}) are much higher than the value reported by Simsek et al.[9] for the same fraction of GNP. This difference can be ascribed to better exfoliation of the graphite by means of the sonotrode under the optimized conditions, and probably by an improved distribution of graphene in our elaborated composites as well.

Figure 7d shows the σ(f) curves recorded at different temperatures (20-195°C) for the composite AYC2.5GSO. Whatever the temperature level, the σ of this composite does not depend on the frequency, revealing then a resistive behavior over the whole explored frequency (10^{-1} - 10^{6} Hz) and temperature (20-195°C) ranges. σ increases as the temperature raised and reaches 2.82 S.cm^{-1} at 195°C.

Finally, since the GNP particles are two-dimensional, σ was otherwise monitored on a bar cut from the SPS-sintered composite AYC2.5GSO in the directions parallel ($\sigma_{//}$) and perpendicular ($\sigma_{\perp}$) to the applied pressing axis (Inset of Figure 7e). Figure 7e presents the recorded conductivities $\sigma_{//}$ and $\sigma_{\perp}$ versus frequency at 20°C for this composite. It evidences that the GNP entailed an anisotropy therein with a ratio ($\sigma_{\perp}$ / $\sigma_{//}$) = 4.4, stemming from the fact that they were oriented, under the effect of uniaxial pressure during the SPS sintering, in the direction perpendicular to the pressing axis. Indeed, since GNP particles possess the superior

σ in their in-planes over that of their out-planes, they induce $\sigma_{\perp}$ larger than $\sigma_{//}$ within the composite AYC2.5GSO.

4. Conclusions

Graphene nanoplatelets were incorporated in AlN-based ceramics comprising sintering additives of Y_2O_3 and CaF_2. SPS process combined to the multiple preparation configuration allowed to produce full densified (>99%) ceramic composites with three samples per SPS cycle, enabling the assemenet of reproductibility and significant time and energy savings.

Their electrical conductivity was demonstrated to be tuned by acting on the exfoliation process. More efficient exfoliation leads to increased number of graphene monolayers with higher charge carrier mobility. The electrical conductivity reaches 10^{-4} S.cm^{-1} for composite containing 2.5 vol.% NGP, i.e. 10 order of magnitude higher as compared to the commercial AlN ceramics. The fine tuning of the electrical conductivity through graphene incorporation is suitted for many other systems.

Acknowledgements

The authors thank the National Research Fondation (ANR, ASTRID program) for funding.

4. References

1 N. Chasserio, S. Guillemet-Fritsch, T. Lebey and S. Dagdag, Ceramic substrates for high-temperature electronic integration, *J. Electron. Mater.*, 2009, **38**, 164–174.

2 Y.-D. Yu, A. M. Hundere, R. Høier, R. E. Dunin-Borkowski and M.-A. Einarsrud, Microstructural characterization and microstructural effects on the thermal conductivity of AlN (Y_2O_3) ceramics, *J. Eur. Ceram. Soc.*, 2002, **22**, 247–252.

3 J. C. González, M. Á. Rodríguez, I. A. Figueroa, M.-E. Villafuerte-Castrejón and G. C. Díaz, Development of AlN and TiB_2 composites with Nb_2O_5, Y_2O_3 and ZrO_2 as sintering aids, *Materials*, 2017, **10**, 324.

4 X. He, F. Ye, H. Zhang and Z. Zhou, Study on microstructure and thermal conductivity of spark plasma sintering AlN ceramics, *Mater. Des.*, 2010, **31**, 4110–4115.

5 Y. Xiong, Z. Fu and H. Wang, Microstructural effects on the transmittance of translucent AlN ceramics by SPS, *Mater. Sci. Eng. B*, 2006, **128**, 7–10.

6 S.-X. Song, Z. Wang and G.-P. Shi, Heating mechanism of spark plasma sintering, *Ceram. Int.*, 2013, **39**, 1393–1396.

7 L. Qiao, H. Zhou, H. Xue and S. Wang, Effect of Y_2O_3 on low temperature sintering and thermal conductivity of AlN ceramics, *J. Eur. Ceram. Soc.*, 2003, **23**, 61–67.

8 H. Nakano, K. Watari and K. Urabe, Grain boundary phase in AlN ceramics fired under reducing N_2 atmosphere with carbon, *J. Eur. Ceram. Soc.*, 2003, **23**, 1761–1768.

9 I. N. G. Simsek, A. Nistal, E. García, D. Pérez-Coll, P. Miranzo and M. I. Osendi, The effect of graphene nanoplatelets on the thermal and electrical properties of aluminum nitride ceramics, *J. Eur. Ceram. Soc.*, 2017, **37**, 3721–3729.

10 C. Yun, Y. Feng, T. Qiu, J. Yang, X. Li and L. Yu, Mechanical, electrical, and thermal properties of graphene nanosheet/aluminum nitride composites, *Ceram. Int.*, 2015, **41**, 8643–8649.

11 C. Lee, X. Wei, J. W. Kysar and J. Hone, Measurement of the elastic properties and intrinsic strength of monolayer graphene, *Science*, 2008, **321**, 385–388.

12 Y. Fan, L. Wang, J. Li, J. Li, S. Sun, F. Chen, L. Chen and W. Jiang, Preparation and electrical properties of graphene nanosheet/Al_2O_3 composites, *Carbon*, 2010, **48**, 1743–1749.

13 C. Ramirez, F. M. Figueiredo, P. Miranzo, P. Poza and M. I. Osendi, Graphene nanoplatelet/silicon nitride composites with high electrical conductivity, *Carbon*, 2012, **50**, 3607–3615.

14 T. Kusunose, T. Sekino and K. Niihara, Production of a grain boundary phase as conducting pathway in insulating AlN ceramics, *Acta Mater.*, 2007, **55**, 6170–6175.

15 B. Román-Manso, Y. Chevillotte, M. I. Osendi, M. Belmonte and P. Miranzo, Thermal conductivity of silicon carbide composites with highly oriented graphene nanoplatelets, *J. Eur. Ceram. Soc.*, 2016, **36**, 3987–3993.

16 J. D. Renteria, S. Ramirez, H. Malekpour, B. Alonso, A. Centeno, A. Zurutuza, A. I. Cocemasov, D. L. Nika and A. A. Balandin, Strongly anisotropic thermal conductivity of free-standing reduced graphene oxide films annealed at high temperature, *Adv. Funct. Mater.*, 2015, **25**, 4664–4672.

17 H. Xia, X. Zhang, Z. Shi, C. Zhao, Y. Li, J. Wang and G. Qiao, Mechanical and thermal properties of reduced graphene oxide reinforced aluminum nitride ceramic composites, *Mater. Sci. Eng. A*, 2015, **639**, 29–36.

18 A. Reina, X. Jia, J. Ho, D. Nezich, H. Son, V. Bulovic, M. S. Dresselhaus and J. Kong, Layer area, few-layer graphene films on arbitrary substrates by chemical vapor deposition, *Nano Lett.*, 2009, **9**, 3087–3087.

19 A. Guermoune, T. Chari, F. Popescu, S. S. Sabri, J. Guillemette, H. S. Skulason, T. Szkopek and M. Siaj, Chemical vapor deposition synthesis of graphene on copper with methanol, ethanol, and propanol precursors, *Carbon*, 2011, **49**, 4204–4210.

20 J. N. Coleman, Liquid-Phase Exfoliation of Nanotubes and Graphene, *Adv. Funct. Mater.*, 2009, **19**, 3680–3695.

21 K. R. Paton, E. Varrla, C. Backes, R. J. Smith, U. Khan, A. O'Neill, C. Boland, M. Lotya, O. M. Istrate, P. King, and others, Scalable production of large quantities of defect-free few-layer graphene by shear exfoliation in liquids, *Nat. Mater.*, 2014, **13**, 624–630.

22 G. Bepete, E. Anglaret, L. Ortolani, V. Morandi, K. Huang, A. Pénicaud and C. Drummond,

Surfactant-free single-layer graphene in water, *Nat. Chem.*, 2017, **9**, 347–352.

Figure caption

Figure 1. **(a)** The prepared solution, containing 2.5 vol.% of graphite powder in 20 ml of isopropyl alcohol, before sonication. **(b)** Images taken immediately after the sonication of this solution for 2 h by using the sonotrode and **(c)** after the sonicated solution was left to settle for 15 h. The volume *Va* (black part of the container) is visibly higher than that of the solution before sonication, indicating the exfoliation of the graphite.

Figure 2. Schematics illustrating the two SPS configurations used for elaborating AlN-based ceramics: **(a)** single and **(b)** multiple preparations. Images of the corresponding single pellet and the stack of three pellets upon SPS treatment are given for each configuration. SEM images of the fracture surfaces obtained by cleavage of the AlN + 3 wt% Y_2O_3 (AY) ceramics, produced in nitrogen atmosphere by SPS at 1800°C under 50 MPa for 10 min, using **(c)** simple preparation and multiple preparation configuration in **(d)** top, **(e)** middle and **(f)** bottom positions.

Figure 3. TEM micrographs of GNP deposited over the TEM grid immediately upon 9h - sonication of a solution containing 2.5 vol.% of graphite in 20 ml of isopropyl alcohol. They show (a) quasi-transparent two-dimensional flakes, and (d) less transparent and thicker flakes comprising a higher number of single-layers.

Figure 4. SEM images of the fracture surfaces obtained by cleavage of the ceramics produced in nitrogen atmosphere by SPS at 1800°C under 50 MPa for 10 min: **(a)** AlN (A) ceramic and **(b)** its corresponding XRD pattern, **(c)** AlN + 3 wt% Y_2O_3 (AY) ceramic and **(d)** its corresponding XRD pattern, and **(e)** AlN + 3 wt%Y_2O_3 + CaF_2 (AYC) ceramic.

Figure 5. SEM images of the fractured surface of the ceramic AlN + 1 wt% Y_2O_3 + 2 wt% CaF_2 + 2.5 vol.% GNP (AYC2.5G) produced by SPS, with the GNP produced using the conventional sonication (ultrasonic bath). **(a)** An overall view showing the distribution of GNP

in the AlN matrix. **(b)** Observation at higher magnification of this microstructure revealing the GNP inserted between the grains forming waves. Inset is the result of the EDS microanalysis indicating the detection of Y, Al, O and Ca elements in the secondary phases concentrated at the triple points between the grains. **(c)** Observation of a thick stack containing a very high number of graphene flacks.

Figure 6. (a) SEM image of the fracture surface of the composite AlN + 1 wt% Y_2O_3 + 2 wt% CaF_2 + 2.5 vol.% GNP (AYC2.5GSO) produced by SPS, with the GNP produced using the the sonotrode. Little GNP observed in the microstructure suggesting the presence of graphene monolayers and GNP containing a very small number of layers invisible by using SEM. Inset: secondary phases YAP and $Ca_3Al_2O_6$ concentrated at grain boundaries. **(b)** Observation at higher magnification of GNP inserted between the grains of the AlN matrix. **(c)** The XRD pattern recorded for this composite.

Figure 7. Frequency dependence of the electrical conductivity $\sigma(f)$ measured at 20°C for the elaborated AIN-based materials. **(a)** AlN ceramic fabricated by SPS (sample A) and the commercial AlN one (from Impak company). **(b)** Composite AlN + 1 wt% Y_2O_3 + 2 wt% CaF_2 + 2.5 vol.% GNP (AYC2.5G) produced by SPS using simple (AYC2.5G) and multiple (AYC2.5G-H (High position) and AYC2.5G-M (middle position)) configurations. For comparison, the curves $\sigma(f)$ recorded for a composite comprising 10 vol.% of GNP (AYC10G) is plotted. GNP incorporated in these samples were produced by exfoliation of graphite in isopropyl alcohol using conventional sonication for 1 h. **(c)** Composites AlN + 1 wt% Y_2O_3 + 2 wt% CaF_2 + 2.5 vol.% GNP produced by SPS using simple (AYC2.5GSO) and multiple (AYC2.5GSO-H, AYC2.5GSO-M, AYC2.5GSO-L) configurations. GNP incorporated in these samples were obtained by exfoliation of graphite in isopropyl alcohol upon sonication for 9 h using the sonotrode. Note that for comparison, the curves σ (f) recorded for the A ceramic and the commercial one (from Impak company) are also plotted in Figure 7b and c. **(d)** σ (f) curves recorded at different temperature levels (20-350°C) for the composite AYC2.5GSO. **(e)** The electrical conductivities $\sigma_{//}$ and $\sigma_{\perp}$ versus frequency measured at 20°C for the AYC2.5GSO composite in the directions parallel ($\sigma_{//}$) and perpendicular ($\sigma_{\perp}$) to the applied pressing axis as illustrated in Inset.

Table caption

Table 1. References of samples prepared and measured in this work. -US* : Ultra Sonic bath

Table 2. The electrical conductivity values recorded at 0.1 Hz and 20°C for the studied samples.

FIGURES

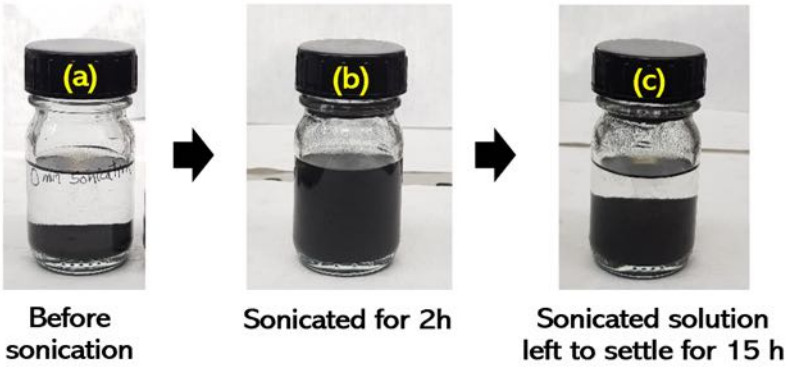

Figure 1

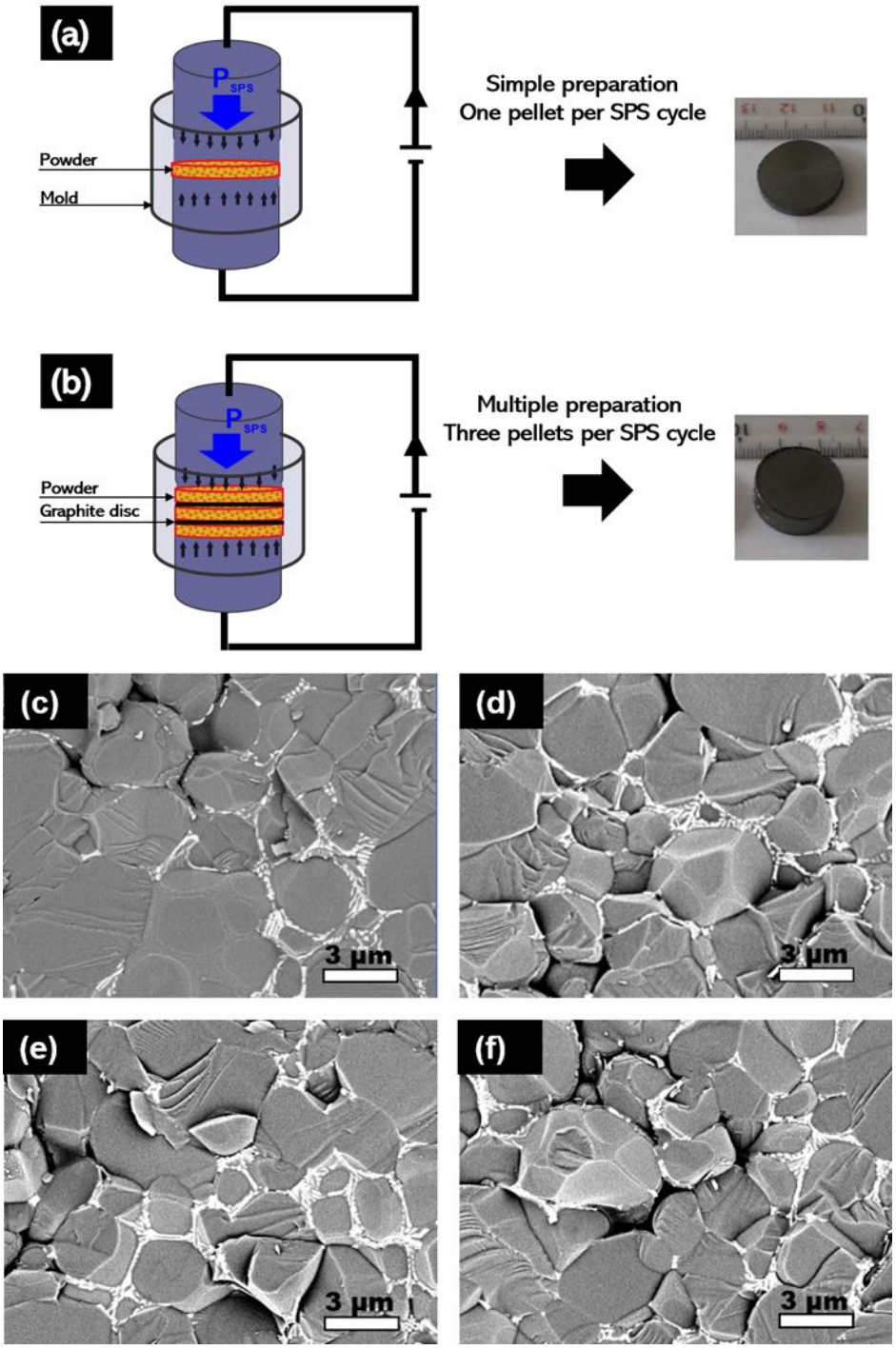
(a)
P SPS
Powder
Mold
Simple preparation
One pellet per SPS cycle
(b)
P SPS
Powder
Graphite disc
Multiple preparation
Three pellets per SPS cycle
(c)
3 μm
(d)
3 μm
(e)
3 μm
(f)
3 μm

Figure 2

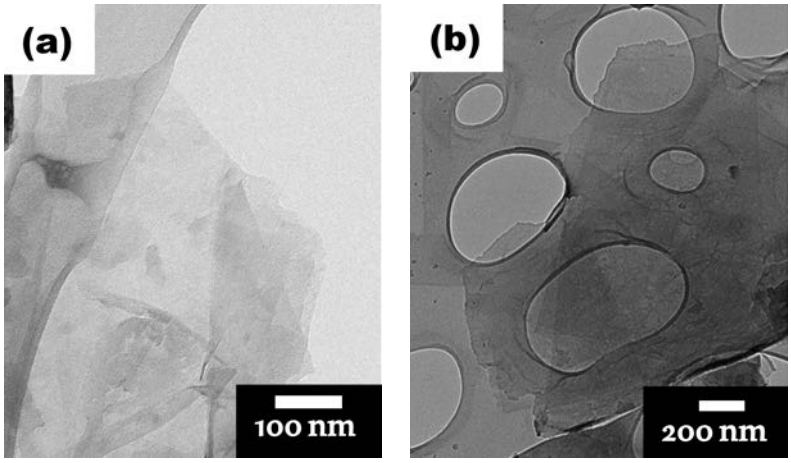

Figure 3

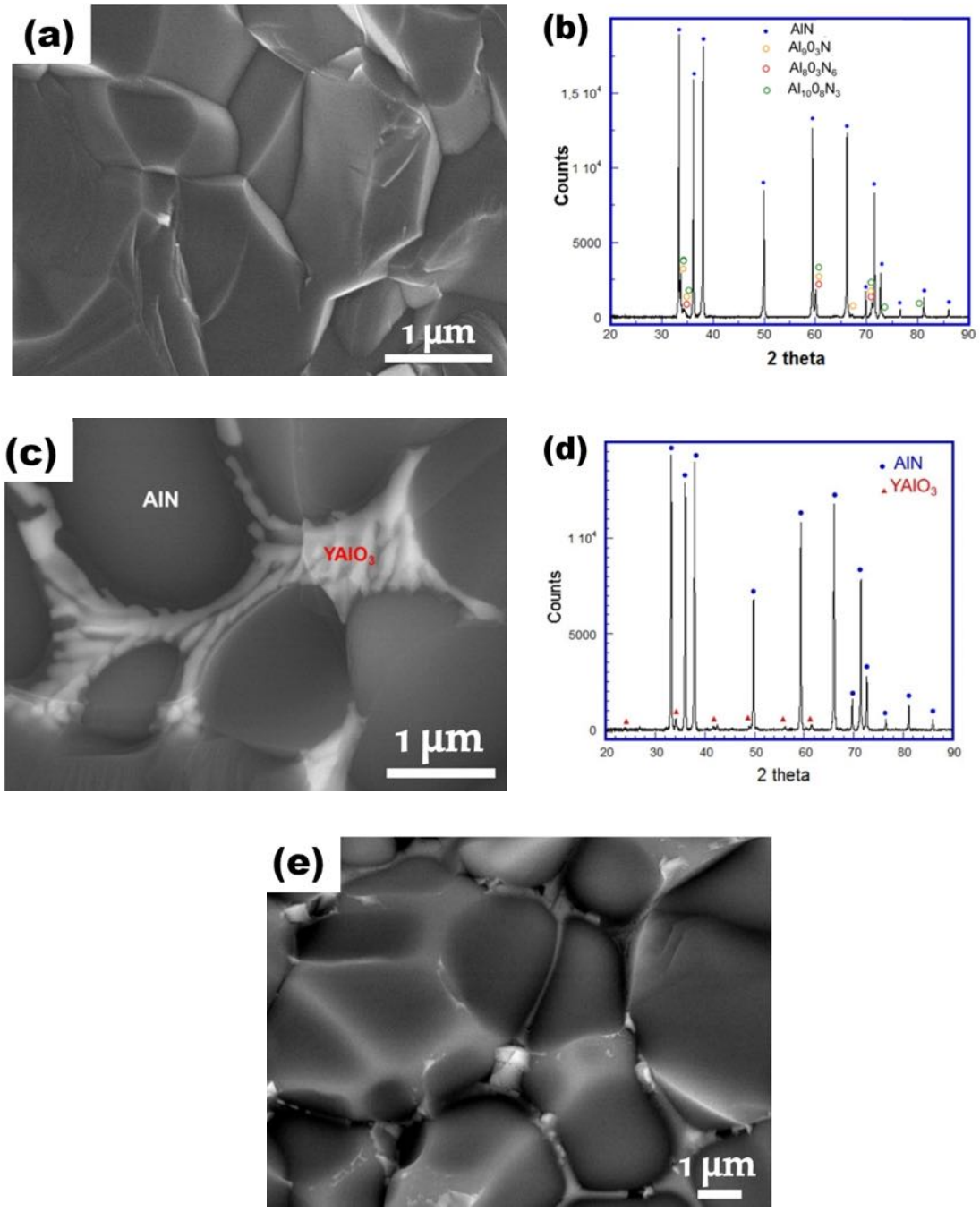
(a)
1 µm
(b)
AlN
Al_9O_3N
$Al_8O_3N_6$
$Al_{10}O_8N_3$
Counts
2 theta
(c)
AlN
$YAlO_3$
1 µm
(d)
AlN
$YAlO_3$
Counts
2 theta
(e)
1 µm

Figure 4

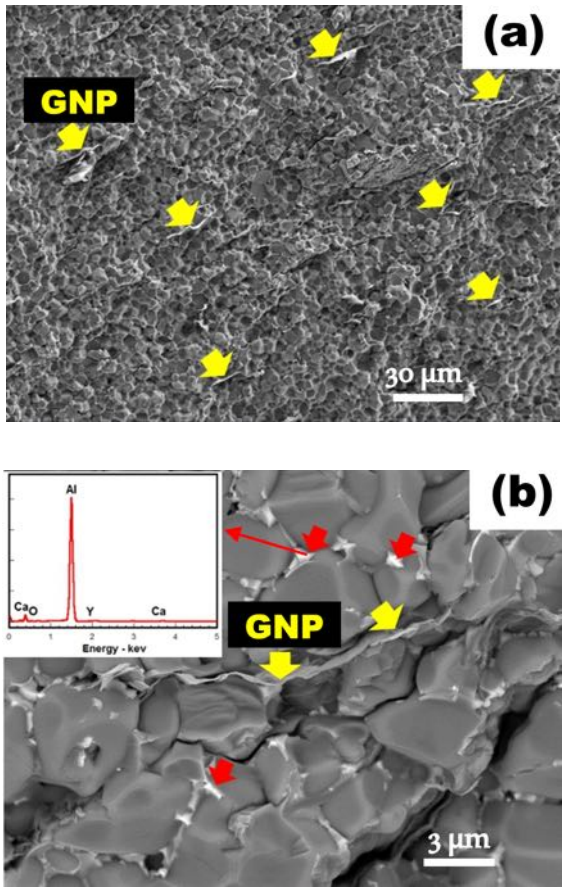

Figure 5

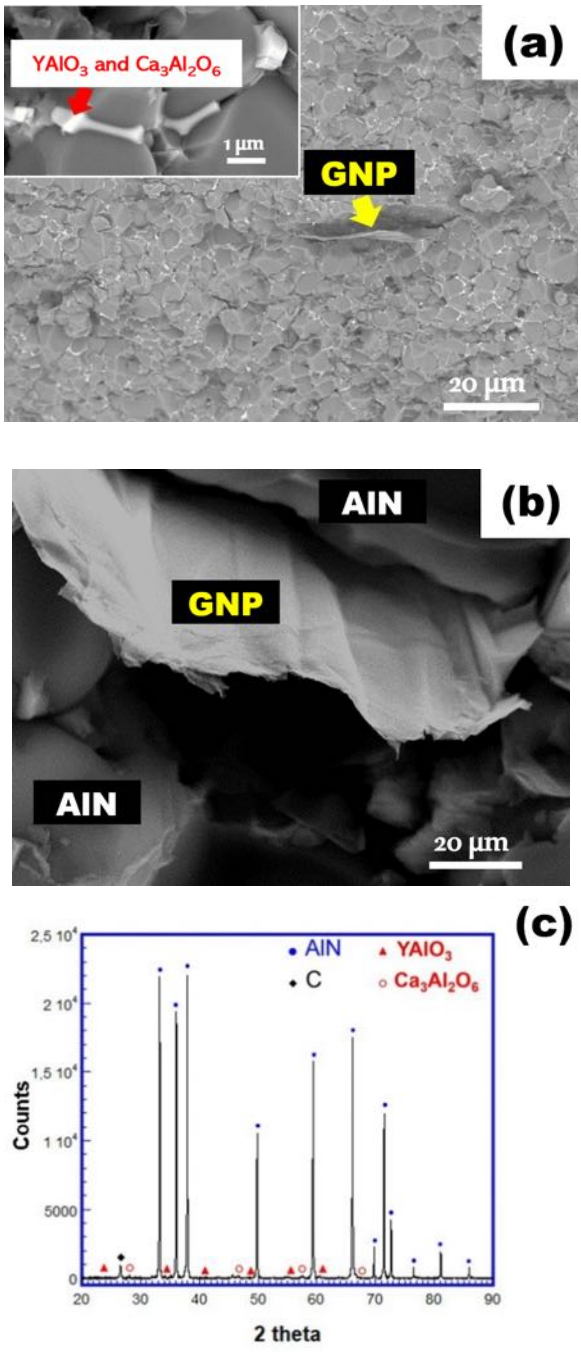
(a)
YAlO3 and Ca3Al2O6
1 µm
GNP
20 µm
(b)
AlN
GNP
AlN
20 µm
(c)
AlN
YAlO3
C
Ca3Al2O6
Counts
2 theta

Figure 6

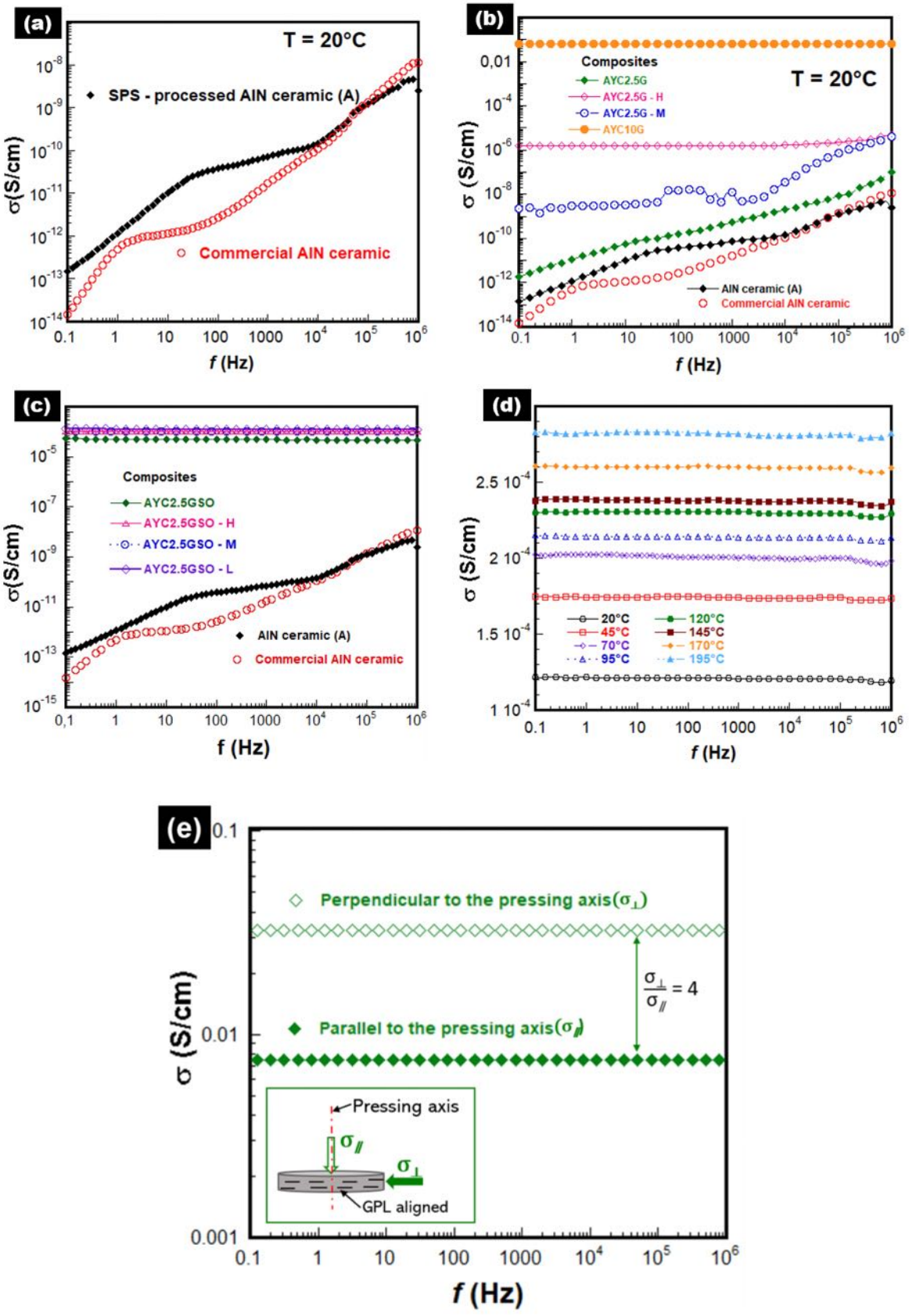
(a)
T = 20°C
SPS - processed AlN ceramic (A)
Commercial AlN ceramic
σ(S/cm)
f (Hz)
(b)
Composites
AYC2.5G
AYC2.5G - H
AYC2.5G - M
AYC10G
T = 20°C
AlN ceramic (A)
Commercial AlN ceramic
σ (S/cm)
f (Hz)
(c)
Composites
AYC2.5GSO
AYC2.5GSO - H
AYC2.5GSO - M
AYC2.5GSO - L
AlN ceramic (A)
Commercial AlN ceramic
σ(S/cm)
f (Hz)
(d)
20°C
45°C
70°C
95°C
120°C
145°C
170°C
195°C
σ (S/cm)
f (Hz)
(e)
Perpendicular to the pressing axis(σ⊥)
Parallel to the pressing axis(σ//)
σ⊥/σ// = 4
Pressing axis
σ//
σ⊥
GPL aligned
σ (S/cm)
f (Hz)

Figure 7

TABLES

Reference	Composition	Vol% GNP	Exfoliation process	Sample configuration during sintering	Density (%)
Impak company	AlN-based ceramic	-	-	-	-
A	AlN	-	-	Single sample	98
AY	AlN+3wt%Y_2O_3	-	-	Single sample	99
AYC	AlN+1wt%Y_2O_3+2wt%CaF_2	-	-	Single sample	99
AYC2.5G	AlN+1wt%Y_2O_3+2wt%CaF_2	2.5	US* (1 h)	Single sample	99
AYC2.5G-H	AlN+1wt%Y_2O_3+2wt%CaF_2	2.5	US* (1 h)	3 samples (High position)	99
AYC2.5G-M	AlN+1wt%Y_2O_3+2wt%CaF_2	2.5	US* (1 h)	3 samples (Middle position)	99
AYC2.5G-L	AlN+1wt%Y_2O_3+2wt%CaF_2	2.5	US* (1h)	3 samples (Low position)	99
AYC10G	AlN+1wt%Y_2O_3+2wt%CaF_2	10	US (1 h)	Single sample	97.8
AYC2.5GSO	AlN+1wt%Y_2O_3+2wt%CaF_2	2.5	Sonotrode (9 h)	Single sample	99
AYC2.5GSO-H	AlN+1wt%Y_2O_3+2wt%CaF_2	2.5	Sonotrode (9 h)	3 samples (High position)	99
AYC2.5GSO-M	AlN+1wt%Y_2O_3+2wt%CaF_2	2.5	Sonotrode (9 h)	3 samples (Middle position)	99
AYC2.5GSO-L	AlN+1wt%Y_2O_3+2wt%CaF_2	2.5	Sonotrode (9 h)	3 samples (Low position)	99

Table 1

			Samples incorporating GNP therein, with GNP produced using ultrasonic bath			
Reference	Impak company	A	AYC2.5G	AYC2.5G-H	AYC2.5G-M	AYC10G
Electrical conductivity, σ ($S.cm^{-1}$) At 0.1 Hz and 20°C	1.5×10^{-14}	1.47×10^{-13}	1.7×10^{-12}	1.5×10^{-6}	2×10^{-9}	6.5×10^{-2}
			Samples incorporating GNP therein, with GNP produced using the sonotrode			
Reference			AYC2.5GSO	AYC2.5GSO-H	AYC2.5GSO-M	AYC2.5GSO-L
Electrical conductivity, σ ($S.cm^{-1}$) At 0.1 Hz and 20°C			10^{-5}	~ 10^{-4}		

Table 2